Isotopic control over self-assembly in supramolecular gels

Kate McAulay,[a] Han Wang,[b] Ana M. Fuentes-Caparrós,[a] Lisa Thomson,[a] Nikul Khunti,[c] Nathan Cowieson,[c] Honggang Cui,[b] Annela Seddon[d,e] and Dave J. Adams[a,*]

a School of Chemistry, University of Glasgow, Glasgow, G12 8QQ, U.K.

b Department of Chemical and Biomolecular Engineering, Whiting School of Engineering, Johns Hopkins University, 3400 North Charles Street, Baltimore, MD 21218, USA

c Diamond Light Source Ltd, Harwell Science and Innovation Campus, Didcot, OX11 0QX, U.K.

d School of Physics, HH Wills Physics Laboratory, Tyndall Avenue, University of Bristol, Bristol, BS8 1TL, U.K.

e Bristol Centre for Functional Nanomaterials, HH Wills Physics Laboratory, Tyndall Avenue, University of Bristol, Bristol, BS8 1TL, U.K.

SUPPORTING INFORMATION

Contents

Experimental Details

Gelators. The gelators used in this study were synthesised using previously reported procedures.[1, 2]

Stock Solutions. Stock solutions (5 mg/mL) were prepared in Falcon Tubes by dissolving 250 mg of gelator in either deionised water or deuterium oxide (D_2O, 99.9% atom % D, Sigma Aldrich), followed by the addition of 0.1 M sodium hydroxide (NaOH, Sigma Aldrich) or 0.1 M sodium deuteroxide (NaOD), prepared from a 40 wt% solution purchased from Sigma Aldrich). The volumes of H_2O, D_2O, NaOH and NaOD used are presented in Table S1. The solutions were stirred at 1000 rpm overnight to allow complete dissolution of the gelator. The pH of each solution was measured and adjusted to pH 11 ± 0.1 with either 0.1 M NaOH or 0.1 M NaOD.

Gelator	Mass of Gelator (mg)	Volume of H_2O or D_2O (mL)	Volume of 0.1 M NaOH or NaOD (mL)
1	250	38	12
2	250	45	5
3	250	45	5
4	250	45	5

Table S1. Components used to make 50 mL of 5 mg/mL gelator.

Gels. Gels were prepared in Sterlin vials (7 mL) by the addition of 2 mL of a stock solution to glucono-δ-lactone (GdL) (16 mg). The vials were gently rotated to ensure completed dissolution of GdL and left to stand overnight. Rheology data was collected 18 hours after the addition of GdL.

pH Measurements. All pH measurements were performed using a FC200 pH probe (HANNA Instruments) with a 6 mm x 10 mm conical tip. The accuracy of the pH measurements is quoted as ± 0.1.

Rheology. Rheological measurements were performed using an Anton Paar Physica MCR101 or MCR301 rheometers. For the frequency sweeps, measurements were carried out directly on gels formed in the Sterlin vials. Frequency sweeps were performed using a cup and vane system under a strain of 0.5 % using a scan range of 1 rad/s to 100 rad/s. Time sweeps were performed using a PP25/S plate with a measuring gap of 1 mm. An angular frequency of 10 rad/s and a strain of 0.5 % were used. To prevent the sample drying out the rim of the plate was sealed with mineral oil (Alfa Aesar).

Cryo-TEM. Cryogenic TEM imaging was performed using a FEI Tecnai 12 TWIN Transmission Electron Microscope, operating at 100 kV. Gels were immediately diluted five times with water to reduce their viscosity and 6 µL of sample solution was placed on a holey carbon film supported on a TEM copper grid (Electron Microscopy Services, Hatfield, PA). All the TEM grids used for cryo-TEM imaging were treated with plasma air to render the lacey carbon film hydrophilic. A thin film of the sample solution was produced using the Vitrobot with a controlled humidity chamber (FEI). After loading of the sample solution, the lacey carbon grid was blotted using preset parameters and plunged instantly into a liquid ethane reservoir precooled by liquid nitrogen. The vitrified samples were then transferred to a cryo-holder and cryo-transfer stage, which was cooled by liquid nitrogen. To prevent sublimation of vitreous water, the cryo-holder temperature was maintained below −170 °C during the imaging process. All images were recorded by a SIS Megaview III wide-angle CCD camera.

Small Angle X-Ray Scattering (SAXS). SAXS was obtained at beamline B21 at the Diamond Light Source. This beamline operates at a fixed energy of 12.4 keV and a camera length of 4.014 m, resulting in a Q range of 0.004 – 0.44 $Å^{-1}$. The samples were manually loaded into borosilicate glass capillaries (Capillary Tube Supplies UK). Measurement times were 15 s for each sample. 14 frames were acquired and averaged. Data were processed using DAWN[3] and a water background was subtracted as a 2D image within the processing pipeline.

Additional data were collected on a SAXSLAB Ganesha 300XL instrument. 70 μL of the solutions as prepared above in H_2O were transferred to a borosilicate glass capillary (Capillary Tube Supplies UK), sealed, and measured for 3600 s in a Q range of 0.007 - 0.25 $Å^{-1}$. Gels were prepared by addition of GdL to the solution in 10 mL glass vials before transfer to the capillary, sealed using a UV curable adhesive (Norland) and allowed to gel overnight. Data were corrected for transmission, absolute intensity and capillary width.

All data were fitted using SASView 4.0.[4] As the length of the scattering objects falls outside of the Q range for the experiment, an arbitrarily long length was introduced into the model and not allowed to refine.

Details of models used for SAXS data fitting:

All data were fitted in SASView 4.0 without further modification to the models. The details of the form factor, P(q) for a cylinder, a cylinder with an elliptical cross section, and a hollow cylinder are outlined below. Detailed information as to the model for a flexible cylinder is given in the references below.

a) Cylinder

The 2D scattering intensity for a cylinder is described by Guinier[5] and is outlined below.

$$P(q,\alpha) = \frac{scale}{V} F^2(q,\alpha).\sin(\alpha) + background$$

and

$$F(q,\alpha) = 2(\Delta\rho)V \frac{\sin\left(\frac{1}{2}qL\cos\alpha\right) J_1(qR\sin\alpha)}{\frac{1}{2}qL\cos\alpha \quad qR\sin\alpha}$$

where α is the angle between the cylinder axis and $\vec{q}$, $V = \pi R^2 L$ and is the particle volume, R is the particle radius, L is the length, Δρ is the scattering length density difference between the scatterer and the solvent, and J_1 is the first order Bessel function.

Therefore, the output for scattering in 1D from randomly oriented cylinders is given by:[5]

$$P(q) = \frac{scale}{V} \int_0^{\pi/2} F^2(q,\alpha).\sin(\alpha) d\alpha + background$$

b) Flexible cylinder

Modelling the scattering function for a worm-like chain (WLC) cannot be done analytically; instead quantitative structural information is found by Monte Carlo simulations of the Kratky and Porod WLC model, taking into account excluded volume effects. The model used within the SASView software has been extensively detailed by Pedersen and Schurtenberger[6] as well as Chen et al.[7]

c) Flexible Elliptical Cylinder

To take into account the scattering from a non-uniform elliptical cross section of a cylinder, the following applies:

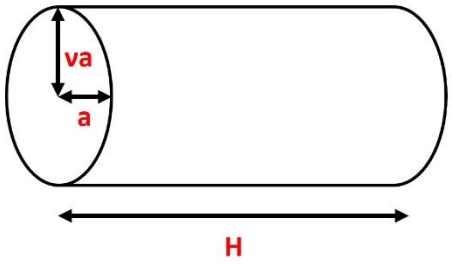

$$\boldsymbol{a = r_{minor}}$$

$$\boldsymbol{\nu = r_{major}/r_{minor} = axis\ ratio}$$

$$I(\vec{q}) = \frac{1}{V_{cyl}} \int d\psi \int d\phi \int p(\theta,\phi,\psi) F^2(\vec{q},\alpha,\psi) \sin\alpha . d\alpha$$

Where $F(\vec{q},\alpha,\psi) = \frac{2J_1(a)\sin b}{ab}$

And $a = qr'\sin\alpha : b = q\frac{L}{2}\cos\alpha : r' = \frac{r_{minor}}{\sqrt{2}}\sqrt{(1+\nu^2)+(1-\nu^2)\cos\psi}$

Ψ is the orientation of the major axis with respect to $\vec{q}$, and α is the angle between the cylinder axis and $\vec{q}$.

For randomly oriented cylinders in 1D, the form factor is averaged over all possible orientations and normalised by volume.

$$P(q) = scale\langle F^2\rangle/V$$

d) Hollow Cylinder

The scattering intensity for a hollow cylinder is described in Guinier, 1955 and is outlined below.

$$P(q) = (scale)V_{shell}\Delta\rho^2\int_0^1 \psi^2\left[q_z, R_{outer}(1-x^2)^{1/2}, R_{core}(1-x^2)^{1/2}\right]\left[\frac{\sin(qHx)}{qHx}\right]^2 dx$$

Where $\psi[q,y,z] = \frac{1}{1-\gamma^2}[\Lambda(qy) - \gamma^2\Lambda(qz)]$

And $\Lambda(a) = 2J_1(a)/a$

$\gamma = R_{core}/R_{outer}$

$V_{shell} = \pi\left(R_{outer}^2 - R_{core}^2\right)L$

$J_1 = (\sin(x) - x.\cos(x))/x^2$

Scale is a scale factor, H = L/2, and J_1 is the first order Bessel function.

Additional SAXS data.

All data had an H_2O or D_2O background subtracted as appropriate. Data for **1** in both H_2O and D_2O in solution fitted as shown previously to a flexible cylinder model with a low Chi squared value, and with values for the radius commensurate with our previous work. As shown previously the length is outside of the Q range for the experiment and was therefore fixed at an arbitrarily high value and not allowed to refine. The gels fitted well to a flexible elliptical cylinder model as has been shown before.

For **2** and **3** in both H_2O and D_2O in solution, we selected a hollow cylinder model based on the TEM images. For **2**, a power law was included to fit the data effectively. In both cases, here the length was allowed to refine and falls into the Q range of the experiment. Comparing this fitted length to the TEM images gives rise to a discrepancy – the TEM data indicates that these hollow tubes are longer than can be probed by this Q range. We postulate that this length is likely to be representative of the Kuhn length, and have observed this behaviour in our previous work.[8] In the gel of **2**, a good fit was found with a flexible elliptical cylinder model. In H_2O, gels of **3** were best described again by a hollow cylinder model where a Schulz polydispersity was required to improve the fit. The length here should be assumed as before to be the Kuhn length of the cylinder rather than its overall length. In D_2O the data fitted best to a flexible elliptical cylinder, showing a clear difference in the gel phase of **3** between H_2O and D_2O. Data for **4** in H_2O was fitted as a flexible elliptical cylinder with an arbitrarily long length. In D_2O a good fit was found fitting to a flexible cylinder. In the gel phase in H_2O, again, a flexible elliptical cylinder best describes the data. However, in D_2O, a cylinder plus a power law was found to be the most appropriate model to describe the gel.

	1 (H_2O)	**1 (D_2O)**	**2 (H_2O)**	**2 (D_2O)**	**3 (H_2O)**	**3 (D_2O)**	**4 (H_2O)**	**4 (D_2O)**
Model	Flexible Cylinder	Flexible Cylinder	Hollow Cylinder + Power Law	Hollow Cylinder + Power Law	Hollow Cylinder	Hollow Cylinder	Flexible Elliptical Cylinder	Flexible Cylinder
Scale	0.0018± 6.3e-5	0.016± 0.0001	0.00073± 1.9e-5	0.066± 0.002	0.021± 0.0002	0.033± 0.0003	0.00036± 1.4e-5	0.063± 0.0009
Background	0.0069± 0.0002	0.0060± 0.0002	0.0096± 0.0006	0.017± 0.0007	0.0052± 0.0002	0.016± 0.0002	0.0088± 0.001	0.012± 0.0004
Radius (Å)	41.1± 0.3	42.8± 0.3	16.6± 0.5	19.0± 0.7	280.7± 0.4	287.1± 0.3	10.53± 1.1	26.0± 0.3
Axis Ratio							3.9± 0.5	
Thickness (Å)			31.9± 0.8	28.3± 1.2	42.5± 0.6	42.9± 0.5		
Kuhn Length (Å)	503.0± 0.03	771.2± 116.3					603.9± 124.7	526.4± 47.9
Length (Å)	>3000	>3000	235.9± 8.8	387.6± 20.0	399.9± 5.3	300.4± 3.0	>3000	>3000
Power law scale			1e-6 *	1e-6*				
Power			2.6	2.0				
Chi Squared	1.60	1.14	1.41	1.83	6.40	11.28	1.02	2.10

(*) Power law scale was not allowed to refine during fitting.

Table S2. Fitting parameters for the solutions of **1**-**4** in H_2O and D_2O.

	1 (H_2O)	**1 (D_2O)**	**2 (H_2O)**	**2 (D_2O)**	**3 (H_2O)**	**3 (D_2O)**	**4 (H_2O)**	**4 (D_2O)**
Model	Flexible elliptical cylinder	Flexible elliptical cylinder	Flexible elliptical cylinder	Flexible elliptical cylinder	Hollow Cylinder	Flexible elliptical cylinder	Flexible elliptical cylinder	Cylinder + Power Law
Scale	0.00060 ± 2.9e-5	0.00054 ± 1.1e-5	0.00025 ± 5.1e-6	0.00024 ± 3.2e-6	3.31e-06 ± 2.2e-9	3.62e-07± 7.4e-10	0.0011 ± 1.7e-5	1.00 e-06 ± 1.0e-8
Background	0.013 ± 0.0002	0.015 ± 0.0002	0.018 ± 0.0002	0.022± 0.0002	3.51e-05± 9.0e-8	2.62e-05± 1.2e-7	0.019 ± 0.0002	1.87 e-05± 3.4e-7
Radius (Å)	25.0 ± 0.72	26.6 ± 0.35	43.0 ± 0.51	46.2 ± 0.56	216.3 ± 0.057	32.3 ± 0.008	28.5 ± 0.25	39.8 ± 0.29
Thickness (Å)					64.9 0.058			
Axis ratio	2.1 ± 0.08	2.2 ± 0.05	3.1± 0.09	3.3 ± 0.06		3.5 ± 0.01	1.9 ± 0.03	
Kuhn Length (Å)	247.3± 0.01	951.3± 170.1	251.4± 20.0	249.3± 21.5		300.0± 32.3	242.0 ± 0.004	
Length (Å)	>1000	>1000	>3000	>3000	248.48± 0.36	>3000	>1000	>3000
Polydispersity (radius)					0.11± 0.0002			
Power Law								3.4e-10± 2.4e-11
Power Law Scale								3.6± 0.01
Chi Squared	1.56	1.06	1.64	2.62	18.17	5.85	2.42	1.15

Table S3. Fitting parameters for the gels of **1**-**4** in H_2O and D_2O.

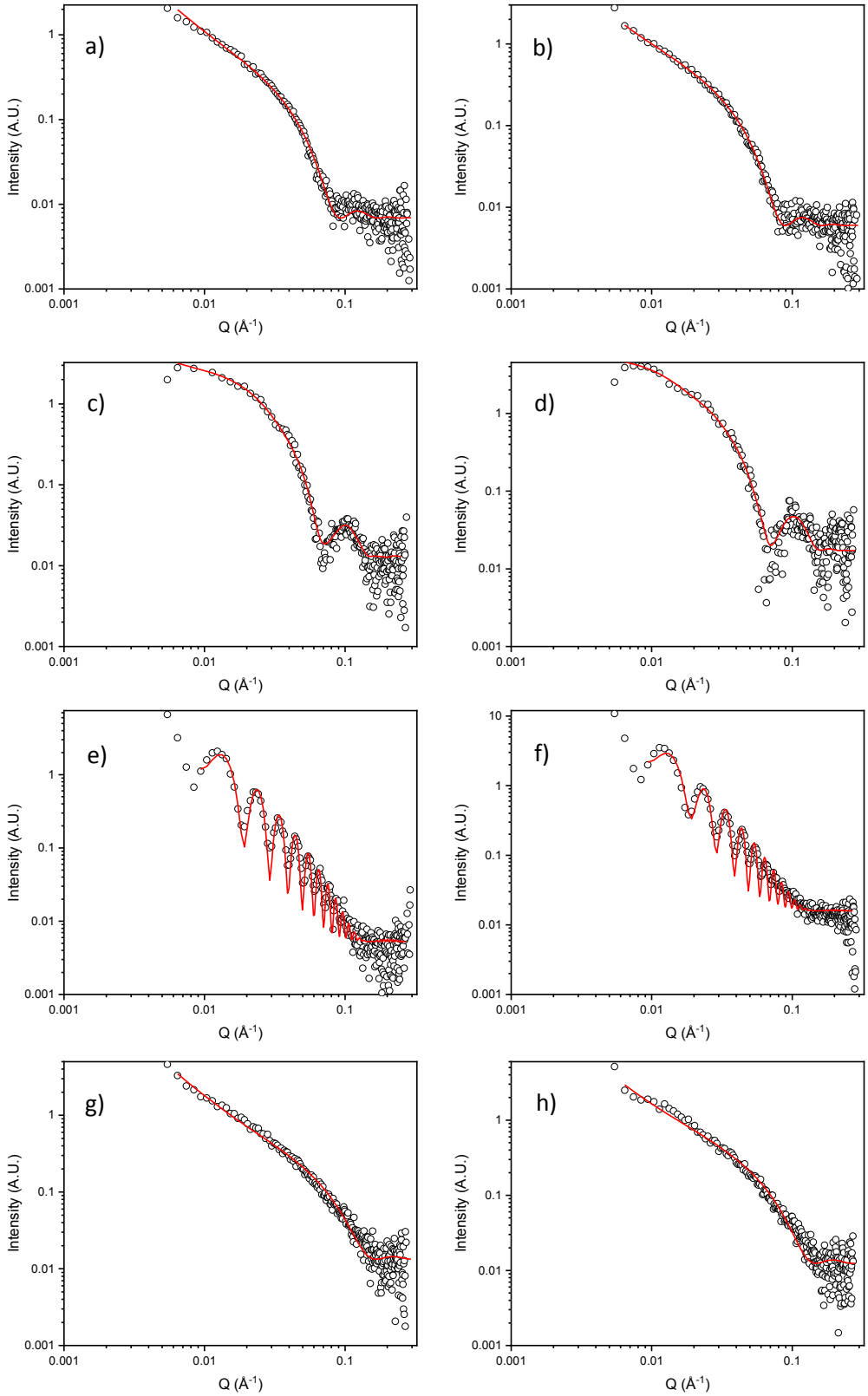

Figure S1. SAXS data for solutions of (a) **1** in H_2O; (b) **1** in D_2O; (c) **2** in H_2O; (d) **2** in D_2O; (e) **3** in H_2O; (f) **3** in D_2O; (g) **4** in H_2O; (h) **4** in D_2O. In all cases, the data are shown as open symbols and the fits as red lines through the data.

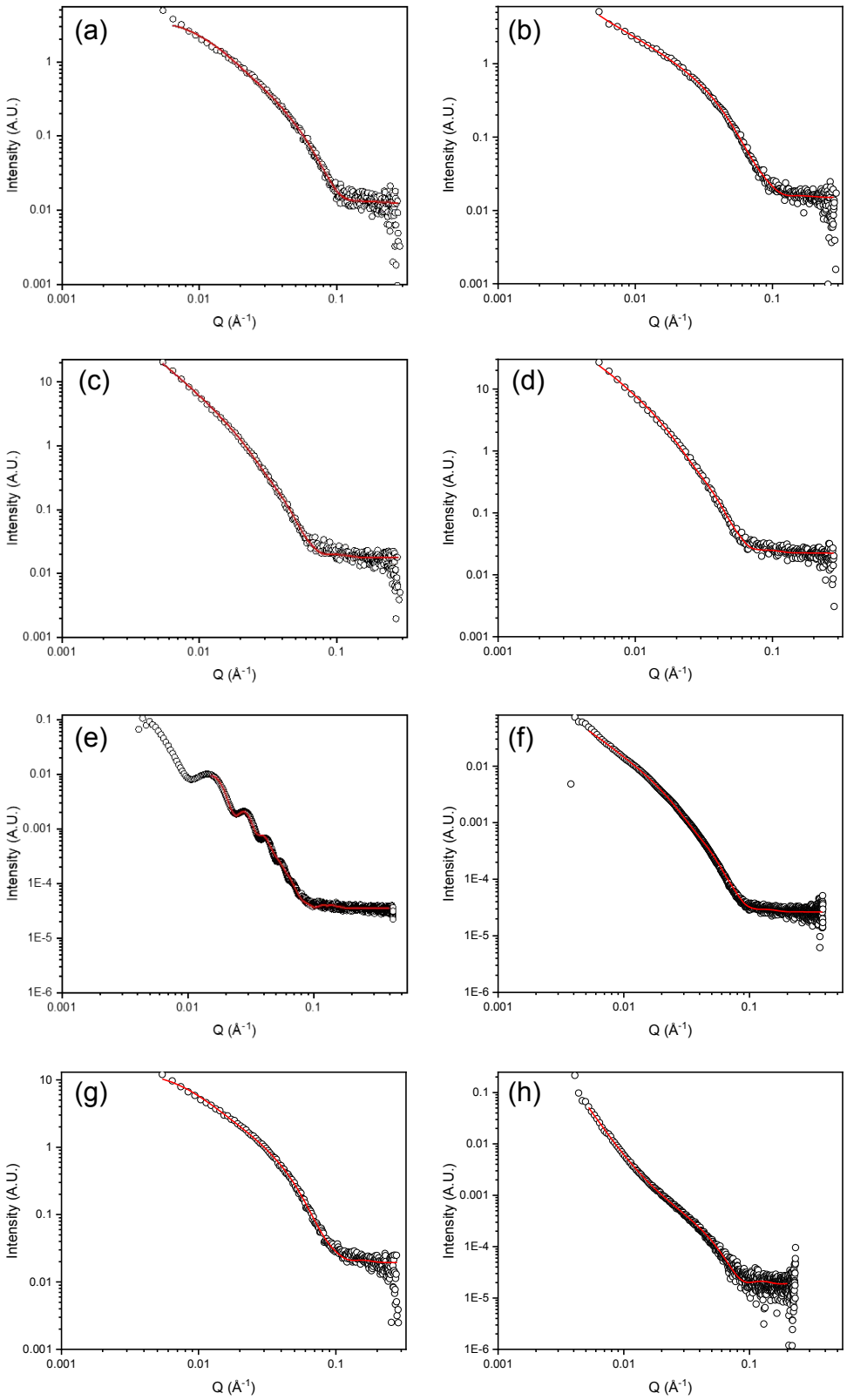

Figure S2. SAXS data for gels of (a) **1** in H_2O; (b) **1** in D_2O; (c) **2** in H_2O; (d) **2** in D_2O; (e) **3** in H_2O; (f) **3** in D_2O; (g) **4** in H_2O; (h) **4** in D_2O. In all cases, the data are shown as open symbols and the fits as red lines through the data.

pH Data

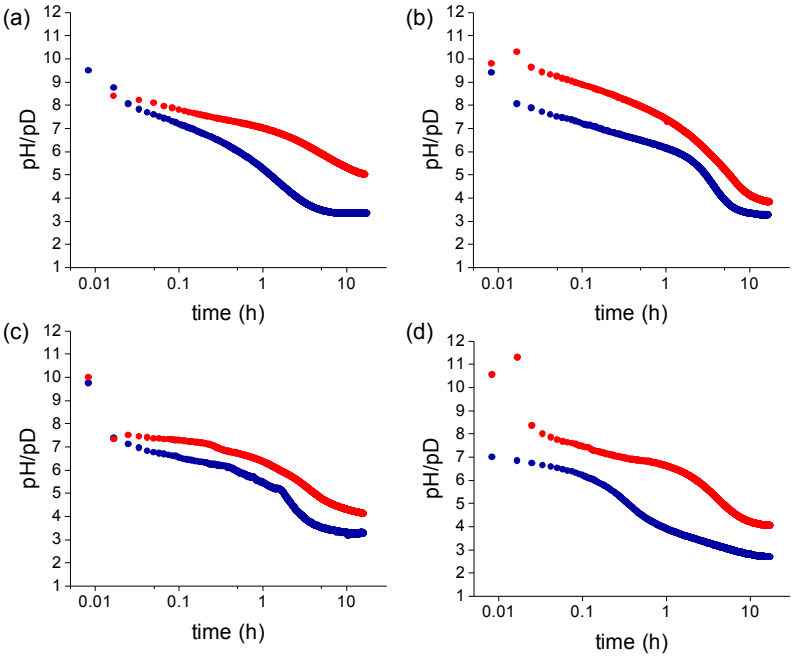

Figure S3. Changes in pH over time after addition of GdL to solutions of (a) **1**; (b) **2**; (c) **3**; (d) **4**. In all cases, the red data are for the solutions in D_2O and the blue data for the solutions in H_2O.

Rheology Data

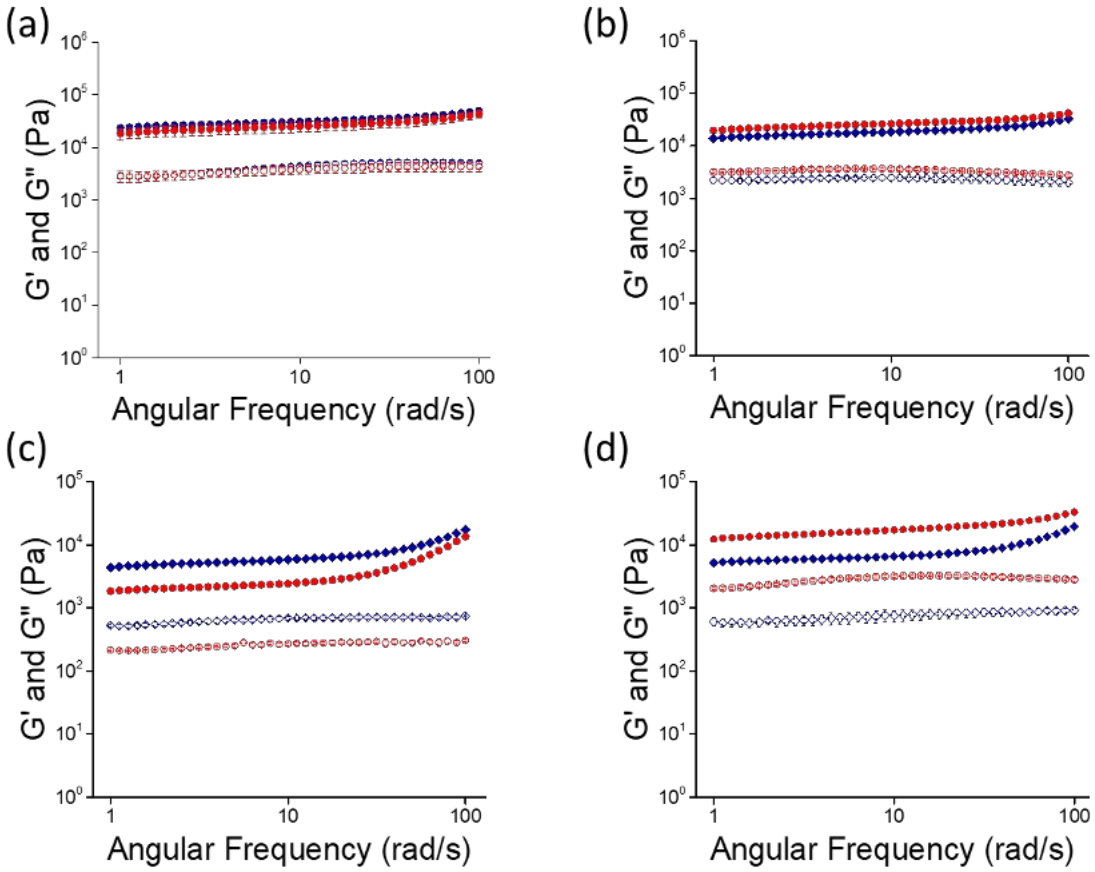

Figure S4. Frequency sweeps for gels formed 18 hours after mixing stock solutions with GdL for (a) **1**; (b) **2**; (c) **3**; (d) **4**. Blue data represents gelation in H_2O and red data shows gelation in D_2O. In both cases, the closed symbols represent G′ and open symbols represent G″. The error bars represent the average of three different measurements on unique gels. Note that there is a weak frequency dependence at low frequency in all cases, as expected for such low molecular weight gels. At higher frequency for 3 and 4, there is an increase in G′ and G″. This is not due to slip since we collected the data using a vane and cup but may be a flow artefact. We note that similar effects are seen using nanoindentation for related gels.[9]

Additional Cryo-TEM data.

To collect these data, a thin film has to be prepared from the gel phase. This is most commonly carried out by pressing the grid on or into the gel and hoping that the structures that adhere represent those forming the network. This can be problematic for the gel phase. Here, we find that the broken structures are observed, with no evidence of a network. This may be due to the structures that adhere to the grid being not part of the network or perhaps structures that break on adherence to the grid of during the blotting process. As such, whilst we provide example cryo-TEM images in Figure S5, we treat them with caution.

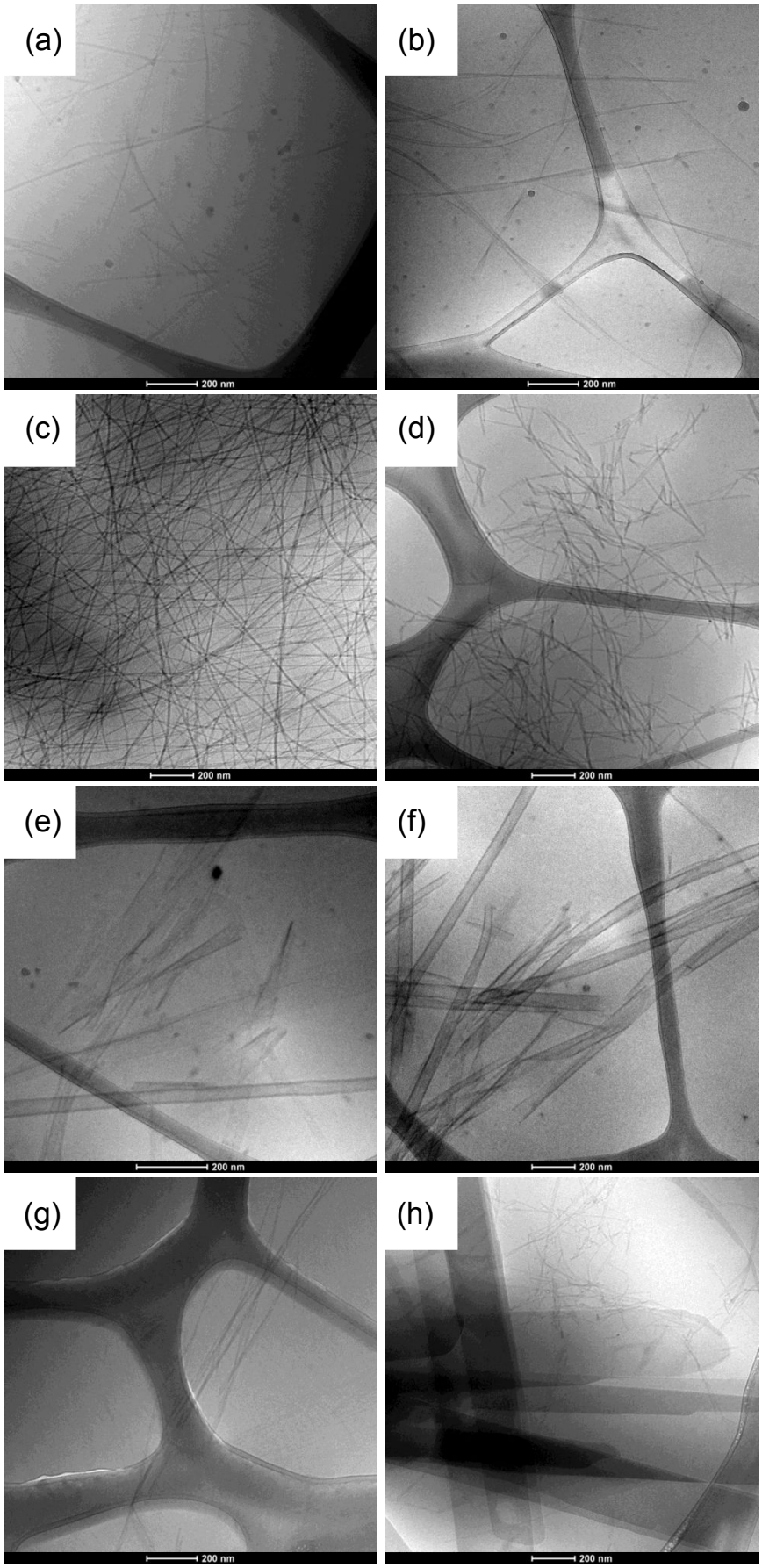

Figure S5. Cryo-TEM data for gels of (a) **1** in H_2O; (b) **1** in D_2O; (c) **2** in H_2O; (d) **2** in D_2O; (e) **3** in H_2O; (f) **3** in D_2O; (g) **4** in H_2O; (h) **4** in D_2O. In all cases, the scale bar represents 200 nm.

References

1. L. Chen, S. Revel, K. Morris, L. C. Serpell and D. J. Adams, *Langmuir*, 2010, **26**, 13466-13471.
2. J. K. Gupta, D. J. Adams and N. G. Berry, *Chemical Science*, 2016, **7**, 4713-4719.
3. J. Filik, A. W. Ashton, P. C. Y. Chang, P. A. Chater, S. J. Day, M. Drakopoulos, M. W. Gerring, M. L. Hart, O. V. Magdysyuk, S. Michalik, A. Smith, C. C. Tang, N. J. Terrill, M. T. Wharmby and H. Wilhelm, *Journal of Applied Crystallography*, 2017, **50**, 959-966.
4. www.sasview.org/.
5. A. Guinier and G. Fourent, *Small angle scattering of X-rays*, John Wiley and Sons, New York, 1955.
6. J. S. Pedersen and P. Schurtenberger, *Macromolecules*, 1996, **29**, 7602-7612.
7. W.-R. Chen, P. D. Butler and L. J. Magid, *Langmuir*, 2006, **22**, 6539-6548.
8. K. McAulay, B. Dietrich, H. Su, M. T. Scott, S. Rogers, Y. K. Al-Hilaly, H. Cui, L. C. Serpell, Annela M. Seddon, E. R. Draper and D. J. Adams, *Chemical Science*, 2019, **10**, 7801-7806.
9. R. Akhtar, E.R. Draper, D.J. Adams and J. Hay, *J. Mater. Res.*, **2018**, 33, 878-883.